Preparation of low-cost ceramic membranes using Persian natural clay and their application for dye clarification

S. Foorginezhad, M.M. Zerafat*

Faculty of Advanced Technologies, Nano-Chemical Engineering Department, Shiraz University, Shiraz, Iran, Tel. +989131965029, email: sahar.foorgi@yahoo.com (S. Foorginezhad), Tel. +989173100957, email: mmzerafat@shirazu.ac.ir (M.M. Zerafat)

ABSTRACT

Low-cost disk-shaped microfiltration membranes were fabricated through uniaxial dry compaction of Iranian natural clays under low pressing pressures (25–150 bar). Water flux, permeability and retention experiments were conducted using a dead-end setup at a low transverse pressure (0.1 bar) via controlling the fluid height above the membrane. Acid yellow 49, basic violet 16 and disperse red 167 dyes were considered for filtration as anionic, cationic and nonionic dyes, respectively. Filtration experiments showed that VI, VIII and IX membranes have the highest flux rate. Membrane IX pressed under 50 bar with 27% porosity and 2491.4 $L \cdot m^{-2} \cdot h^{-1} \cdot bar^{-1}$ permeability represented the highest retention; 98% anionic and 93% nonionic and no significant (~20%) cationic dye retention. Zeta potential analysis illustrated the negative membrane charge in dye solutions. Scanning electron microscopy (SEM) micrographs confirmed that the as-prepared porous crack-free membranes is suitable candidate for microfiltration applications. Moreover, the as-prepared membrane showed higher flux and lower shrinkage compared with the membrane fabricated using commercial montmorillonite (MMT). Based on the results, the low-pressure membranes fabricated using natural clays can be used for dye fractionation with almost no energy consumption.

Keywords; Microfiltration; Natural clay; Dye removal; Low pressure membrane

1. Introduction

Due to low energy consumption, cost effective manufacturing process and no chemical additives, membrane technology has received a great deal of attention in separation industries. In recent years, application of ceramic membranes is prevailing the organic counterparts due to thermal, mechanical and chemical resistance and also ease of fabrication. Utilization of abundant materials as additives or even starting materials, leads to cost-effective fabricated membranes. Generally, several research activities on ceramic membranes have been focused on alumina [1–5] both as the support and also the main separation layer in a composite structure [6–8]. In other studies, titania [9,10], silica [11,12] and zirconia [13] have also been reported. However, high processing expenses and sintering temperatures have limited their application in industrial scale. Therefore,

utilization of low-cost materials with high performance is necessary for large-scale applications. Recently, research studies have been directed toward abundant raw materials such as clays [14] and clay-based materials like kaolin [15], montmorillonite (MMT) [16], mullite [17], apatite [18] and cordierite [19], etc. In addition to natural abundance and low price, these materials are sintered at relatively lower temperatures, while exhibiting high thermal, mechanical and chemical stability. Moreover, various utilized pore formers reported in several studies like starch [20,21], calcium carbonate [22,23] and sawdust [24,25], show the vast membrane performance.

Nowadays, growth of textile industry has led to increase the introduction of dye containing effluents into the environment. Incomplete attachment of dyes onto the fabrics results in their release as a secondary effluent [26]. Dyes are synthetic aromatic compounds comprising of various organic and metallic functional groups. Acid dyes are used for silk, wool, leather and nylon, basic dyes for modified

*Corresponding author.

polyester, nylon and polyacrylonitrile and disperse dyes for cellulose acetate, nylon and cellulose are various types which are commonly used in textile industry [27].Generally, discharge of dye containing effluents without proper treatment cause serious environmental pollution with harmful effects on human, animals and plants [26]. As a result, refining dye containing effluents before discharge into the environment needs special attention.

Treatment of dye containing effluents through membrane separation technology is one of the promising and commercially available processes which can replace other removal techniques such as oxidation [28], photo-catalysis [29,30] and adsorption [31,32]. Microfiltration (MF) membranes with pores in the 0.1–10 µm range [33] are commonly used for separation of microorganisms and suspended particles from aqueous media, also concentration and purification in various fields such as textile, pharmaceutical, food and chemical industries [33,34]. Dye removal, separation of oil-water emulsions and suspended particles are also considered using MF membranes [35]. Several studies have been directed toward the fabrication of MF membranes using low cost materials. Recently, Bouazizi et al. [36], prepared flat ceramic MF membranes using natural bentonite with a 520 L·m^{-2}·h^{-1}·bar^{-1} permeability. Clarification of colored textile effluents was performed using a dead-end filtration setup at 0.1 bar. The transverse pressure required for filtration was controlled by the fluid height in a separating funnel. The elaborated MF membrane with 1.7 µm mean pore size performed almost total discoloration and elimination of suspended solids. Palacio et al. [37] fabricated a flat ceramic MF membrane using clay and phosphate for filtration of murexide, methyl orange and potassium chromate. All filtration tests were performed at 0.015 bar. Around 30–40% methyl orange and potassium chromate and also 60% murexide retention was reported. Yun et al. [38], fabricated asymmetric Al_2O_3 MF membranes using polymethylmethacrylate (PMMA) as pore former. According to the results, almost complete suspended solid and colloidal elimination was obtained at a 0.08 bar transmembrane pressure. Mouiya et al. [39], fabricated flat ceramic MF membranes using natural clay with phosphate as pore former through uniaxial pressing under 150 MPa. The as-prepared membrane with a 2.5 µm pore size and 28.11% porosity was considered for industrial and synthetic wastewater treatment under 0.14 bar. According to the results, almost total turbidity removal and significant discoloration was observed. Also, it was concluded that the as-prepared membrane showed strong alkaline and poor acid resistance. Saja et al. [40], elaborated flat MF membranes through uniaxial pressing of natural perlite and starch as pore former under 795 bar. The optimized membranes with 52.11% porosity and 1.7 µm pore size were considered for industrial wastewater filtration. According to the results, 97 and 96% turbidity retention was observed for agro-food and tannery effluents, respectively. Majouli et al. [41], prepared flat MF membranes through extrusion of local Moroccan perlite. Various organic additives were used as plasticizer, binder, lubricating and porosity agents in order to elaborate crack-free membranes with a 6.64 µm average pore size and 41.8% porosity. Membranes represented 95–100% removal for turbidity from baking powder suspension under a 0.11 bar transmembrane pressure. The as-prepared membranes

represented good chemical stability in acidic media, but 6wt.% loss was observed in alkaline media.

In the present study, low cost flat MF membranes were fabricated using natural clay minerals collected from Fars region (Iran) through uniaxial pressing under low pressures in the 25–150 bar range. It was observed that the as-prepared membranes permeation started at ~0.05 bar. Consequently, filtration experiments were conducted through controlling the height of water above the membrane with no external energy requirement. Water flux, permeability, chemical resistance, porosity and shrinkage measurements were performed. Membranes with higher permeability were considered for filtration of disperse red 167, acid yellow 49 and basic violet 16 as non-ionic, anionic and cationic dyes. The optimal membrane with the highest dye retention was characterized by zeta potential and mercury porosimetry techniques. Moreover, in order to investigate the efficiency of membranes fabricated using natural clays and compare them with commercial clay membranes, several flat disks were prepared using commercial MMT. The as-prepared membranes indicated promising water flux and dye rejection at a~0.1 bar transmembrane pressure.

2. Experimental

2.1. Materials and methods

2.1.1. Materials

Clay minerals (samples I-IX) were collected from Fars region (Iran). Raw clays were crushed and sieved through sieve No. 25 (<6 µm particles). Nano-clay (MMT) was purchased from Nanosany Co. (Mashhad province, Iran). Polyethylene glycol (PEG, 400 Mw) was purchased from Merck Co. Basic violet 16 ($C_{23}H_{29}ClN_2$), Acid yellow 49 ($C_{16}H_{13}Cl_2N_5O_3S$) and disperse red 167 ($C_{23}H_{26}ClN_5O_7$) were provided from a local textile workhouse. Dye characteristics are shown in Table 1. Gyration radius, which can be defined as the distance of any point in an object parting from its center of mass was calculated for dyes using visual molecular dynamic (VMD) software. The obtained values were in agreement with dye radius calculated through empirical techniques given by Gordon and Chambers [42].

2.1.2. MF membrane preparation

Membranes were fabricated through mixing each natural clay minerals with organic additives. The optimal formulation of precursors was selected according to experimental results. According to Table 2, each clay mineral was homogeneously mixed with various amounts of PEG as binder in a mortar. Then, the blended mixtures were placed in a disk-shaped stainless-steel mold and uni-axially pressed. To investigate the effect of membrane compaction pressure on filtration, mixtures were pressed under various uni-axial pressures in the 25–150 bar range. For initial formation and homogeneous drying [43,44], the as-prepared raw flat disks with 1.9 cm diameter and 2 mm thickness were maintained in open air for 24 h and then sintered at 1100°C for 3 h at a 1°C/min heating rate. Furthermore, in order to compare the performance of membranes fabricated using natural clay with those fabricated with commercial clay, several mem-

Table 1
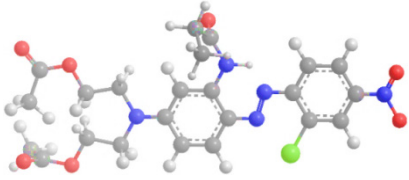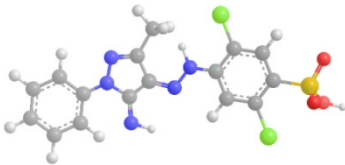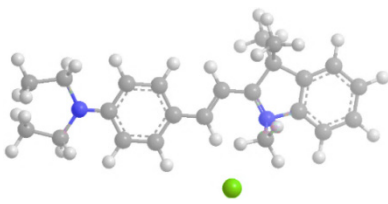Dye characteristics considered for microfiltration using the as-prepared MF membranes

Name	M_w (g/mol)	Chemical formula	Chemical property	Molecular structure	Gyration radius (A°)
Disperse Red 167	519.93	$C_{23}H_{26}ClN_5O_7$	Non-ionic		5.547
Acid Yellow 49	448.26	$C_{16}H_{13}Cl_2N_5O_3S$	Anionic		5.195
Basic Violet 16	368.94	$C_{23}H_{29}ClN_2$	Cationic		5.185

Table 2
Composition of raw materials used for the MF membrane fabrication

Clay minerals (wt.%)	PEG (wt.%)	Pressing pressure (bar)
100	–	25–150
95	5	
90	10	
85	15	
80	20	

branes were prepared using commercial MMT mixed with PEG and with the optimal compositions previously determined for natural clay minerals. Also, the flowchart given in Fig. 1, presents the main steps of MF membrane fabrication.

2.1.3. Characterization

Cumulative and density distribution of clay minerals and MMT were evaluated and measured by *particle size distribution (PSD)* using dynamic light scattering (DLS) particle size analyzer (JAPA Horiba LB550). Chemical composition of clay minerals were evaluated using *X-ray fluorescence (XRF)* analysis via PW1410 (PHILIPS Co., Netherland). *Mercury intrusion porosimetry* (Thermo Finnigan, Pascal 440) was performed in order to determine the pore size distribution of MF membrane based on the intrusion of mercury into the pores as a function of the applied pressure. Surface morphology and structural analysis of the optimal membrane before and after filtration was characterized using *scanning electron microscopy (SEM)* micrographs taken

byVEGA3 TESCAN apparatus. Membrane surface charge was qualitatively specified using *Zeta potential measurement* (MicotracZetaCheck). *Mechanical strength* of membranes was evaluated through compression experiment using a micro-hardness tester (MH1, KOOPA Co.). Chemical stability was evaluated by weight loss of membranes immersed in extreme acidic (pH = 2) and alkaline (pH = 13) solutions using H_2SO_4 and NaOH, respectively as a function of time.

Filtrate concentration was determined using Beer-Lambert:

$$A = \varepsilon lc \tag{1}$$

where A is the absorbance measured using *UV-visible spectrophotometer* (UV-1280, Shimadzu), ε the molar absorptivity or molar extinction coefficient (L·mol^{-1}·cm^{-1}), l length of light path (cm) and c the solution concentration (mol·L^{-1}).

Apparent porosity of the membranes was also measured via water absorption using Archimedes technique [45]. Briefly, membranes were weighed before and after water absorption, where open pore volume (V_{op}) corresponds to volume of water absorbed. Volume of absorbed water can be calculated using membrane mass difference before and after water absorption:

$$V_{op} = m_s - m_d \tag{2}$$

where m_s and m_d are membrane weight after and before water absorption (g), respectively. Open porosity can be calculated using:

$$\%Open\ porosity = \frac{V_{op}}{V_a} \times 100 \tag{3}$$

where V_{op} and V_a are open pore and apparent volumes (cm^3), respectively.
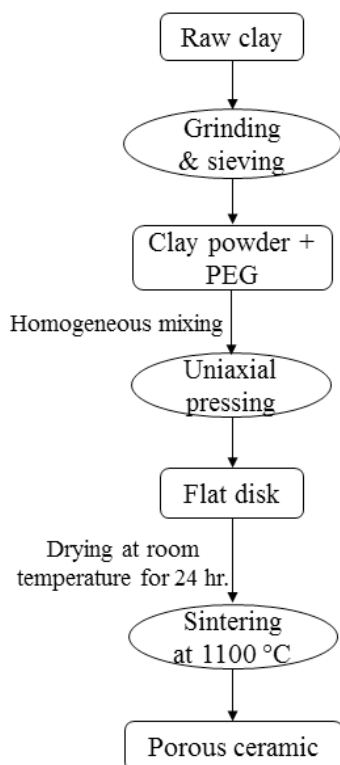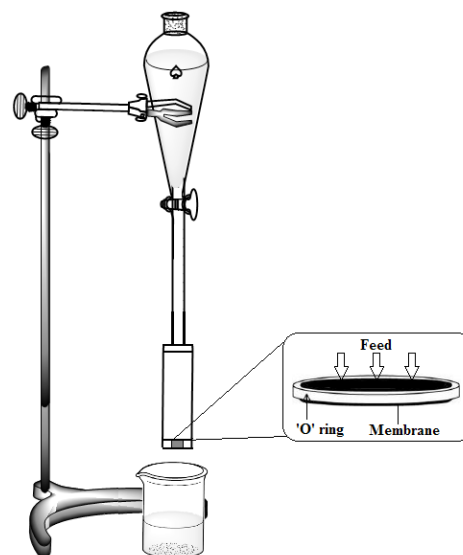
Fig. 1. Schematic diagram of membrane fabrication main steps.

Fig. 2. Laboratory scale device for dead-end filtration tests using the as-prepared MF membranes.

2.1.4. Filtration test

Filtration experiments were conducted using a laboratory scale dead-end setup (Fig. 2). Membranes were immersed in deionized water for 24 h prior to filtration. According to Fig. 2, the setup consists of a stainless-steel tube with a cylindrical top part and a base plate as the membrane housing. The membrane is sealed in the plate with an 'O' ring. The feed solution is filled in the tubular section above the membrane from the top and the transmembrane pressure is applied by controlling the height of liquid between the membrane surface and level of liquid in the separating funnel. Filtration experiments were conducted under 0.1 bar (1.1 m liquid height), through collecting the permeate at various time intervals. Water flux (J) was measured under 0.1 bar as a function of specific surface area and permeate volume collected during a specified time interval according to [46]:

$$J = \frac{Q_w}{\Delta t \cdot A_m} \tag{4}$$

where J is water flux (L·m^{-2}·h^{-1}), Q_w permeate volume (L), Δt sampling time (h) and A_m the membrane specific surface area (m^2). Also, membrane permeability was measured in the 0.05–0.2 bar range [40]:

$$L_p = \frac{J}{\Delta p} \tag{5}$$

where L_p is the membrane permeability (L·m^{-2}·h^{-1}·bar^{-1}), J water flux (L·m^{-2}·h^{-1}) and Δp the transmembrane pressure (bar).

2.1.5. Microfiltration of dye solutions

Membrane performance regarding dye filtration was measured using retention tests. Filtration experiments were applied at a constant pressure of 0.1 bar. Acid yellow 49, basic violet 16 and disperse red 167 dye solutions in the 20–50 ppm range were intended as the feed solution. Filtrate concentration was measured using a UV-Visible spectrophotometer and retention is measured according to [37]:

$$\%R = \left[1 - \left(\frac{C_p}{C_0}\right)\right] \times 100 \tag{6}$$

where R is retention and C_p and C_0 are permeate and feed concentrations (here mol·L^{-1}), respectively.

3. Results and discussion

3.1. Characterization of raw materials

3.1.1. MMT

Chemical composition of MMT is given in Table 3. It can be observed that MMT consists of SiO$_2$ and Al$_2$O$_3$ in general with traces of sodium, potassium, magnesium, titanium, calcium and iron oxides. Also, MMT particle size as cumulative and density distributions are given in Fig. 3. According to the data, MMT represents a uni-modal population distribution in the 0.131–0.669 μm range with a 0.332 μm mean value. The majority of particles (~81.38%) are located between 0.259 μm and 0.445 μm. Also, reddish brown color of the sintered membrane is related to iron oxidation [16].

3.1.2. Clay minerals

Table 4 indicates the chemical composition of natural minerals collected from Fars region. As can be seen, minerals consist of various amounts of metal oxides which can

affect the sintering temperature and consequently mechanical strength. According to the literature review performed and empirical results, in order to achieve a porous structure with sufficient mechanical strength, higher sintering temperatures are required for membranes fabricated using clays with higher Al_2O_3 contents (sintered at 1300–1400°C). On the other hand, low sintering temperatures are favored for reduction of energy consumption. As a result, all clay samples were considered for fabrication of MF membrane with sufficient porosity and mechanical stability at low sintering temperatures. According to Table 4, it can be concluded that SiO_2 and Al_2O_3 are the main components with similar values of titanium, magnesium, calcium, sodium and potassium oxides, but various iron oxide contents. It was found that, the higher iron oxide content leads to the formation of darker membranes through thermal treatment. It can be concluded that, IX and VIII samples with the lowest Al_2O_3 content can be sintered at lower temperatures. Figs. 4a–i indicate PSD for each clay mineral based on cumulative and density distributions. Fig. 4a reveals the size distribution of sample I located in the range of 1–6 μm and 1.9 μm mean size with almost 76% of particles <2 μm. Based on the PSD analysis of sample III, particles are located in the range of 0.669–6 μm with a 2.116 μm mean size (Fig. 4c). Size distribution of sample IV shown in Fig. 4d, represents two separate size distribution. Almost 80.67% of particles are located in 0.039–0.067 μm and 19.33% in the 3.9–6 μm range. Fig. 4e depicts the sharp distribution of sample V in the 2.6–6 μm size range with a 4.44 μm mean size. Fig. 4f illustrates the unimodal and sharp distribution of sample VI. According to the data, particles are located in the range of 4.472–6 μm with a 5.498 μm mean size and ~93.87% of particles are ~6 μm. According to Figs. 4g,h and b, the VII, VIII and II samples are in a similar range of 1.3–6 μm with 2.7, 2.4 and 2.7 μm mean size, respectively. Also, Fig. 4i describes the PSD of sample IX. As can be seen, particles are located in the 0.877–6 μm range with a 2.707 μm mean size. Around 63% of the particles are <3 μm and 37% are in the 3–6 μm size range.

Table 3
Chemical composition of commercial MMT (wt. %) using XRF analysis

Composition	wt.%
Na_2O	0.98
MgO	3.29
Al_2O_3	19.60
SiO_2	50.95
K_2O	0.86
CaO	1.97
TiO_2	0.62
Fe_2O_3	5.62
LOI[a]	15.45

a = loss on ignition
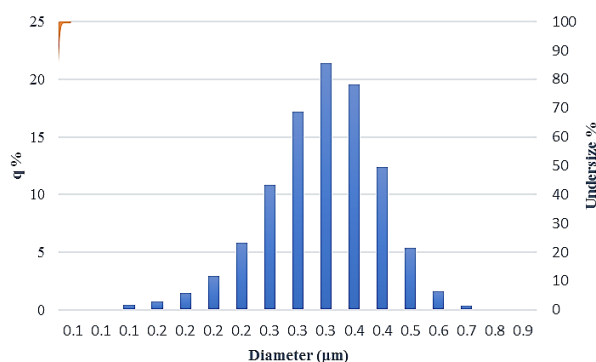
Fig. 3. Particle size distribution (PSD) analysis of MMT using DLS technique [16].

3.2. Characterization of MF membranes

3.2.1. Membrane preparation

The optimal composition was determined by varying the amount of PEG as binder. Typically, according to Table 2, each clay mineral was homogeneously mixed with various amounts of PEG, and placed in a disk-shaped mold and uni-axially pressed under 25–150 bar. It was observed that the membranes fabricated without PEG, indicated large surface cracks and were easily broken. But, increasing the PEG content up to 10 wt.% led to complete elimina-

Table 4
Chemical composition of clay minerals (wt. %) using XRF analysis

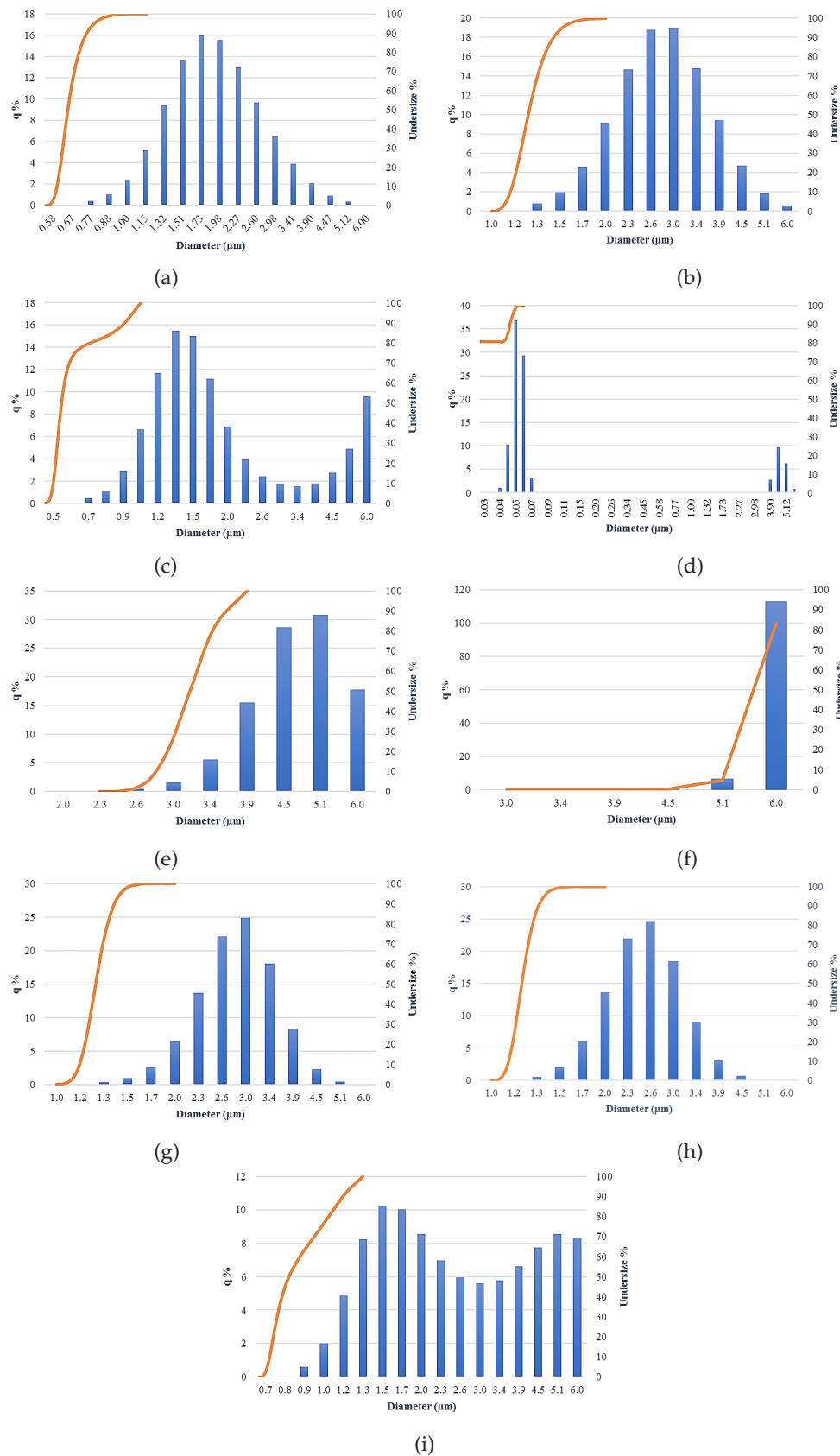|	SiO_2	Al_2O_3	Fe_2O_3	TiO_2	CaO + MgO	$Na_2O + K_2O$	LOI[a]
I	< 63	30	< 1	< 1.5	< 1	3–4	5.5–7.5
II	< 63	30	< 2	< 1.5	< 1	3–4	5.5–7.5
III	< 63	29	< 2	< 1.5	< 1	3–4	5.5–7.5
IV	< 60	< 28	3–5	< 1.5	< 1	3–4	5.5–7.5
V	< 60	< 28	5–8	< 1.5	< 1	3–4	5.5–7.5
VI	< 60	< 26	8–11	< 1.5	< 1	3–4	5.5–7.5
VII	< 57	< 26	11–13	< 1.5	< 1	3–4	5.5–7.5
VIII	< 55	< 25	13–16	< 1.5	< 1	3–4	5.5–7.5
IX	< 50	< 23	>16	< 1.5	< 1	3–4	5.5–7.5

a = loss of ignition

Fig. 4. Particle size distribution (PSD) analysis of (a) I, (b) II, (c) III, (d) IV, (e) V, (f) VI, (g) VII, (h) VIII, (i) IX samples using DLS technique.

tion of surface cracks. On the other hand, further increase in PEG concentration caused membrane deformation. Also, sintered membranes exhibited many small surface cracks. So, the mixture composed of 90 wt.% clay mixed with 10 wt.% PEG was considered as the optimal composition for membrane fabrication. Pure water flux measurement was conducted and membranes with the highest flux rates were selected for dye filtration tests. Consequently, the most efficient membrane with the highest retention rates was considered for further characterizations.

3.2.2. Water flux and permeability

Higher water fluxes under low transverse pressures are usually preferred due to correlation with low energy consumption. Fig. 5 represents the pure water flux of natural clays and commercial MMT membranes under 0.1 bar as a function of uniaxial pressing pressure. According to the graph, water flux tends to decrease as the pressing pressure is increased and, except membrane No. I which shows almost no significant change in flux compared with other membranes, the reduction rate is more severe in the 25–50 bar range. Furthermore, the inset shows the flux of membranes pressed under 50 bar. As can be seen, membranes No. IX, VIII and VI represent the highest water fluxes at 25 and 50 bar; thus, considered for further characterizations. Also, water permeability of IX, VIII and VI membranes pressed under 25 and 50 bar was measured as a key parameter for characterizing membrane capacity in filtration process. Typically, pure water flux was measured as a function of transverse pressure in the 0.05–0.2 bar range and results are shown in Figs. 6a and b. Moreover, it was observed that the water flux was stabilized after ~120 min. According to Figs. 6a and b, it can be clearly seen that water flux experiences a linear increase with the operating pressure. Also, it can be found that the membranes pressed under 25 bar show higher flux rates compared with 50 bar pressed membranes. Furthermore, average permeabilities of IX, VIII and VI membranes pressed under 25 and 50 bar determined using distilled water are shown in Table 5. As can be seen, relatively higher values were obtained for membranes pressed under 25 bar.

3.2.3. Dye retention experiments

Due to the higher flux rates, membranes No. IX, VIII and VI pressed under 25 and 50 bar were considered for dye filtration in the 20–50 ppm range. For initial screening, a 50 ppm disperse red 167 solution was considered for filtration and permeate fluxes shown in Table 6. As can be seen, membrane No. VIII shows the highest flux rates in both pressing pressures.

Furthermore, Fig. 7 shows the permeate flux and dye retention of membranes No. IX, VIII and VI pressed under 25 and 50 bar at a 0.1 bar transverse pressure. It can be observed that, membranes pressed under 25 bar show the highest permeate flux and the lowest dye retention which can be attributed to the larger pore sizes. On the other hand, flux rates tend to decrease and dye retention increase as the pressing pressure is increased up to 50 bar, which can be related to smaller pore sizes. In case of disperse red 167 (non-ionic dye), separation would be performed through
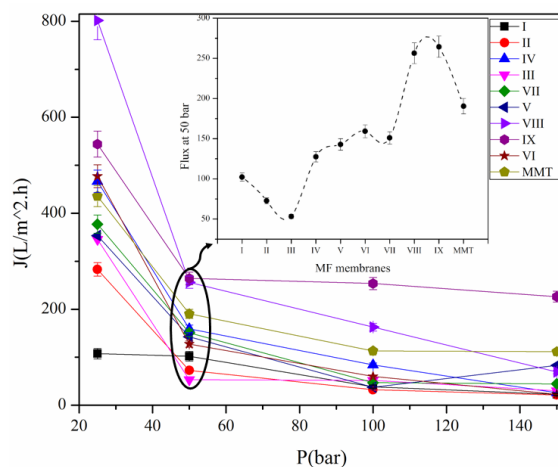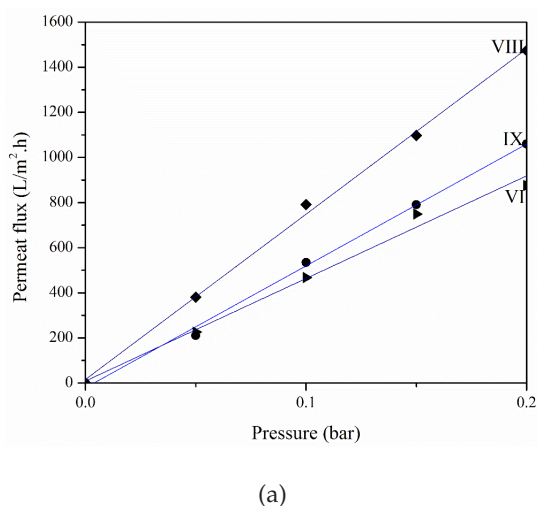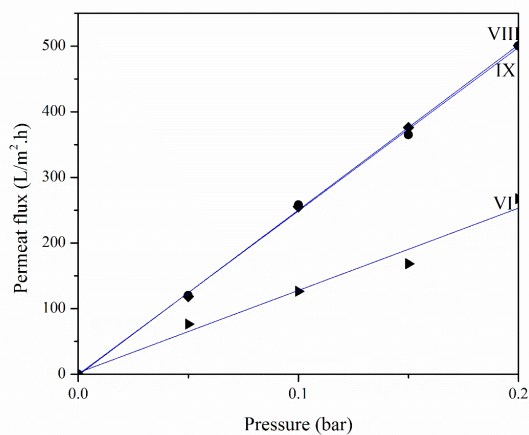

Fig. 5. Pure water flux of (I–IX & MMT) membranes as a function of uniaxial pressing pressure in 25–150 bar range. The inset picture shows the flux of all membranes pressed under 50 bar.

(a)

(b)

Fig. 6. Permeate water flux of VI, VIII and IX membranes pressed under (a) 25 & (b) 50 bar pressure as a function of transverse pressure in the 0.05–0.2 bar range.

Table 5
Average permeability of IX, VIII and VI membranes pressed under 25 & 50 bar using distilled water

Membrane	Pure water permeability (L/m²·h·bar)		
Pressing pressure (bar)	VI	VIII	IX
25	4595.8	7325.1	5402.4
50	1254.2	2501.5	2491.4

Table 6
Permeate fluxes of disperse red 167 microfiltration under 0.1 bar operating pressure using VI, VIII and IX membranes pressed under 25 and 50 bar

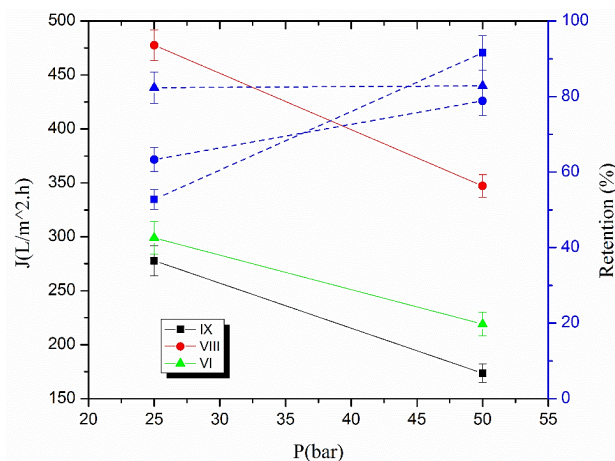| Membrane	Permeate flux (L/m²·h)		
Pressing pressure (bar)	VI	VIII	IX
25	299.08	477.51	277.74
50	219.1	347.2	173.633

Fig. 7. Permeate flux and retention rate of disperse red 167 solution filtration under 0.1 bar transverse pressure using membranes No. IX, VIII and VI pressed under 25 and 50 bar.

size exclusion. So, it can be seen that IX membrane pressed under 50 bar shows ~91.55% dye retention with a 173.633 L/m²·h flux rate. Also, membrane No. VI shows almost a constant 82% dye retention at both pressures, while its flux decrease from 299.08 to 219.1 L/m²·h. In terms of quality, Fig. 8 shows the elimination of 50 ppm disperse red 167 dye solution using membranes No. IX, VIII and VI pressed under 25 and 50 bar at 0.1 bar operating pressure. It is obvious that, dye removal would be increased by increasing the pressing pressure. Consequently, membrane No. IX pressed under 50 bar was considered for further dye retention experiments due to the highest dye retention.

Also, acid yellow 49 and basic violet 16 were selected to investigate the as-prepared MF membrane behavior towards anionic and cationic dyes, respectively. Typically, 50 ppm of each dye solution were filtered using membrane No. IX pressed under 50 bar. The high rejection value can be attributed to the strong interactions between dye molecules and charged surface of the membrane [14] and also size exclusion. In case of acid yellow 49, ~80% removal was obtained during the first 20 min. Then removal reached ~90% and remained constant. This can be attributed to the formation of a thin dye layer on the membrane surface which caused increasing the removal rate by ~10%. The high retention rates agree with the electrostatic repulsion and exclusion of acid yellow anions outside of the negatively charged pores [14] in addition to steric exclusion. In case of basic violet 16, complete discoloration was obtained at initial filtration period. After ~5 min, no significant removal could be observed. According to negative charge of the membrane, this behavior can be explained by two subsequent mechanisms. The initial rejection can be attributed to adsorption of cationic dye onto the membrane surface. While, membrane saturation and equilibrium state after a specified time can lead to surface charge alteration and failing the adsorption; thus, reducing the rejection rate. Figs. 9a and b show acid yellow 49 and basic violet 16 removal qualitatively. Furthermore, membrane No. IX was considered for filtration of 20–50 ppm acid yellow 49 and disperse red 167 dyes. Typically, several solutions in the 20–50 ppm range were prepared and considered for filtration. It should be noted that, all experiments were conducted at batch condition and the permeate was returned to the feed solution cell after each sampling. Also, all filtration experiments were conducted at 0.1 bar trans-
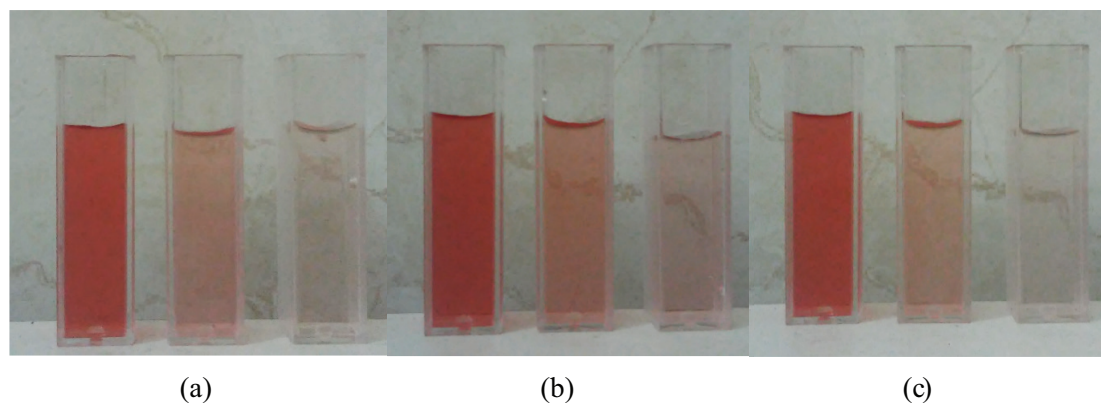

Fig. 8. 50 ppm disperse red 167 dye solution filtration using membranes No. (a) VI, (b) VIII & (c) IX pressed under 25 and 50 bar. From left to right, images indicate initial 50 ppm solution and permeate of membranes pressed under 25 and 50 bar, respectively.

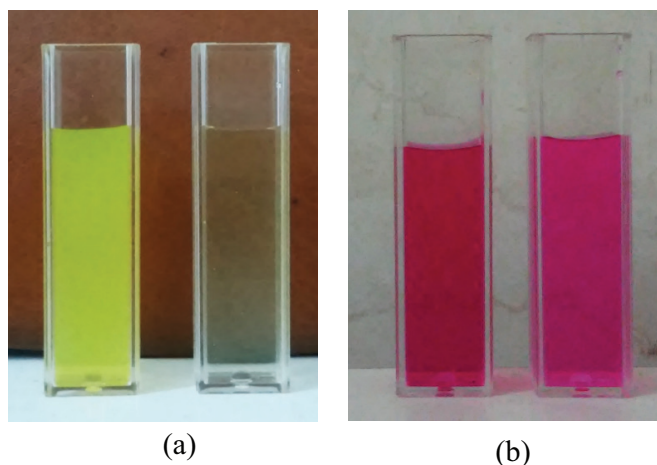(a)   (b)

Fig. 9. Filtration of 50 ppm of (a) acid yellow 49 & (b) basic violet 16 solutions at 0.1 bar operating pressure using membrane No. IX pressed under 50 bar.

verse pressure. So, in order to adjust the operating pressure, fluid height above the membrane was kept constant at 1.1 m by adding feed as makeup. Furthermore, after 4–5 h of dye filtration, the membrane was detached from the system and the dye layer formed on the surface was removed by washing the membrane through immersion in acetone for 1 h. It was observed that the flux and retention rates of treated membranes exhibited no significant change compared to values obtained by the original membrane. According to a reported study [33], continuous decline in flux can be related to fouling, while concentration polarization effect leads to a steady state flow with almost constant flux. Furthermore, batch filtration procedure leads to solute accumulation at the membrane surface and increasing the concentration near the surface cause retention enhancement and flux reduction. A concentration profile built up in the boundary layer, forms a diffusive flow back to the feed bulk. After a steady state achievement, the convective solute flow toward the membrane with diffusive flow back to bulk will be balanced by permeate solute flow through the membrane. The obtained concentration polarization (C_m/C_0) indicates that the flux would be decreased exponentially with logarithm of solute concentration in bulk and the concentrated layer formed near the membrane surface [33].

$$\frac{C_m}{C_0} = \frac{\exp\left(\dfrac{J}{k}\right)}{R_{\text{int}} + \left(1 - R_{\text{int}}\right)\exp\left(\dfrac{J}{k}\right)} \qquad (7)$$

$$R_{\text{int}} = 1 - \frac{C_p}{C_m} \qquad (8)$$

where C_m, C_0 and C_p are solute concentration on membrane surface, feed bulk and permeate, respectively, J is flux, k is mass transfer coefficient and R_{int} is intrinsic retention. In the present study, constant permeate flux after ~120 min can be attributed to concentration polarization. Fig. 10 shows the removal as a function of dye concentration. It can be seen that, acid yellow 49 retention is increased from 80.45% to 98% in the 20–35 ppm range and subsequently tends to decrease to 90% by increasing the concentration up to 50
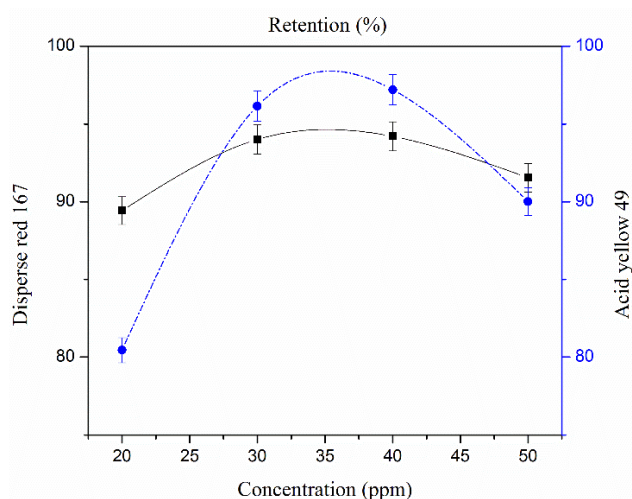

Fig. 10. Retention rate of 20–50 ppm of disperse red 167 and acid yellow 49 solutions filtered at 0.1 bar operating pressure using membrane No. IX pressed under 50 bar.

ppm. In case of disperse red 167, the retention is increased from 89.42% to 93% in the 20–35 ppm range and then decreased to 91.55% at 50 ppm. Form a theoretical point of view, dye retention enhancement can be attributed to pore blocking and formation of a dye layer by increasing the concentration up to the specific value (35 ppm for both dyes). Then, increasing dye concentration leads to increase the diffusion of dye molecules through the concentrated layer formed on the surface, consequently decreasing the retention. Also, permeate flux variation of 35 ppm of disperse red 167, acid yellow 49 and basic violet 16 solutions as a function of filtration time using IX membrane are given in Fig. 11. The results show that the permeate flux decrease by increasing the filtration time. This can be related to accumulation of dye molecules and forming a dye layer on the membrane surface [36,39,40] leading to membrane fouling. Moreover, SEM micrographs of membrane after filtration, confirm this behavior (section 3.2.9). Furthermore, it was found that the lowest flux rates are related to disperse red 167 solution.
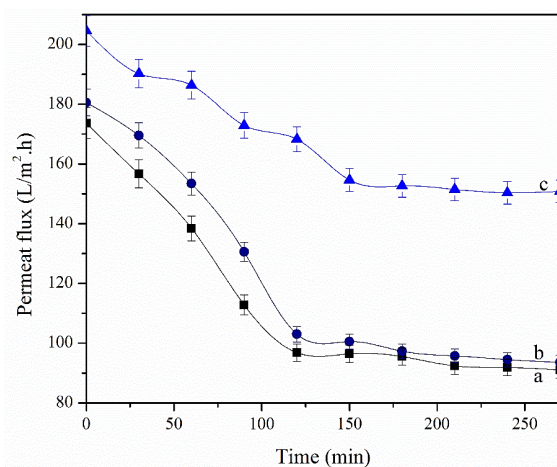
Fig. 11. Variation of permeate flux of 35 ppm of (a) disperse red 167, (b) acid yellow 49 and (c) basic violet 16 solutions at 0.1 bar transverse pressure as a function of filtration time using membrane IX pressed under 50 bar.
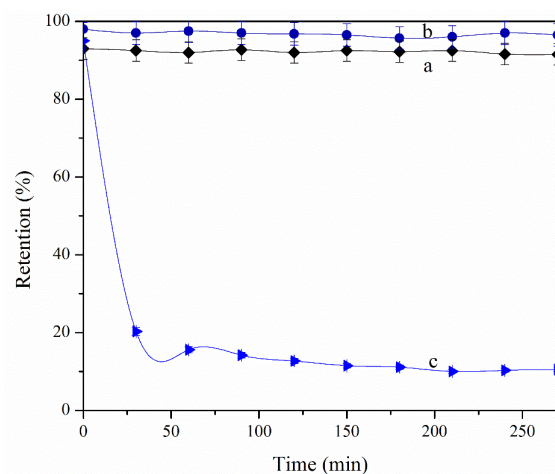

Fig. 12. Variation of retention rate of 35 ppm of (a) disperse red 167, (b) acid yellow 49 and (c) basic violet 16 solutions at 0.1 bar transverse pressure as a function of filtration time using IX membrane pressed under 50 bar.

This can be related to membrane fouling which results in the highest dye retention rate. On the other hand, IX membrane shows the highest permeate flux in case of basic violet 16 filtration which agrees with the lowest membrane fouling and dye retention. Furthermore, IX membrane retention of 35 ppm of disperse red 167, acid yellow 49 and basic violet 16 solutions as a function of filtration time was studied (Fig. 12). It can be found that, only a slight decline in retention rate was observed for disperse red 167 (~1.6%) and acid yellow 49 (~1.53%) during 270 min of filtration which indicates sufficient applicability of the as-prepared membrane for non-ionic and anionic dye filtration, while retention rate of basic violet is sharply decreased by (~88.95%).

3.2.4. Membrane densification

Membranes were prepared with an initial diameter and thickness of 1.9 cm and 2 mm, respectively. Table 7 represents membrane diameters after thermal treatment. According to the results, 5.3–15.8% radial shrinkage with no significant axial shrinkage was observed for clay minerals. Furthermore, commercial MMT membranes showed the highest axial shrinkage which can be attributed to the largest loss on ignition (LOI). Also, Membrane No. IX with 10.5% shrinkage shows the highest densification among clay minerals. Moreover, Fig. 13 shows the view of membranes fabricated using natural clay minerals and also the commercial MMT membrane.

3.2.5. Open porosity

Open porosity of IX, VIII and VI membranes with the highest water flux rates were measured and summarized in Table 8. It can be seen that, the porosity tends to decrease as the pressing pressure enhance. Furthermore, Table 9 presents the median and mean particle size of VI, VIII and IX powders. By comparing Tables 8 and 9, it can be supposed that VI with the highest particle size leads to the highest membrane porosity and more regular arrangement of small particles leads to decrease the porosity of VIII and IX membranes.

Table 7
Membrane densification (%) in terms of radial shrinkage

Sample	Densification (%)	Sample	Densification (%)
MMT	15.8	V	5.3
I	5.3	VI	5.3
II	5.3	VII	5.3
III	5.3	VIII	5.3
IV	5.3	IX	10.5

3.2.6. Chemical stability

Membrane pore blocking leads to a sharp reduction in permeate flux; thus, a regular cleaning procedure is vital. In some cases, membranes are treated in acidic and alkaline solutions which can damage the membrane structure. Consequently, in order to determine the chemical corrosion resistance, membranes were immersed in acidic (H_2SO_4, pH = 2) and alkaline media (NaOH, pH = 13) in various time intervals. The membrane weight was measured as a function of immersion time and results are summarized in Figs. 14a and b. Fig. 14a indicates the membrane weight loss immersed in NaOH. As can be seen, membranes No. VI and I show the highest weight loss of ~4.8%and ~2% during the first 24 h, respectively. Other membranes show no significant weight loss (<0.5%). Weight loss of membranes immersed in H_2SO_4 is also given in Fig. 14b. It was found that, no significant change (<0.5%) in membrane weight was appeared at various time intervals. According to results, it can be seen that the total weight loss in alkaline media is a little higher than acidic media. This can be attributed to the acidic nature of clays resulting in mass loss due to acid-base reactions [36]. On the other hand, IX, VIII and VI membrane were immersed in acidic and alkaline solutions in the pH = 1–14 range prepared using H_2SO_4 and NaOH, respectively and weighed after 14 days of immersion with mean values reported in Fig. 15 as a function of pH. It was observed that, all membranes indicate a similar behavior. It

Fig. 13. View of membranes fabricated using each type of clay.

Table 8
Open porosity of membranes No. VI, VIII and IX pressed under 25 and 50 bar using Archimedes method

| Pressing pressure (bar)	Porosity (%)		
	VI	VIII	IX
25	31.5	31	28
50	29	29	27

Table 9
Median and mean particle size distribution (PSD) of VI, VIII and IX initial powders using PSD analysis statistical data

| PSA analysis	VI (µm)	VIII (µm)	IX (µm)
Median	5.517	2.342	2.205
Mean	5.498	2.388	2.707

can be concluded that, increasing the solution pH up to 14 leads to ~1 wt.% weight loss, while ~0.28 wt.% weight loss is occurred by decreasing the solution pH to 1. Generally, no significant mass loss is observed through acidic and alkaline treatment. Furthermore, it can be seen that the lower mass loss in acidic media shows the better acidic corrosion resistance. The as-prepared membrane stability is in good agreement with fabricated alumina membranes with sufficient chemical resistance in pH = 1–12 [47]. Consequently, the membranes have an acceptable chemical resistance in both acidic and alkaline media.

3.2.7. Surface charge

Due to the highest retention rate of membrane IX, it was selected for zeta potential analysis for determination of the surface charge at original pH of disperse red 167, acid yellow 49 and basic violet 16 dye solutions (pH = 6.5). It was observed that the membrane represents a negative charge (~–48 mV) at the prevailing conditions.
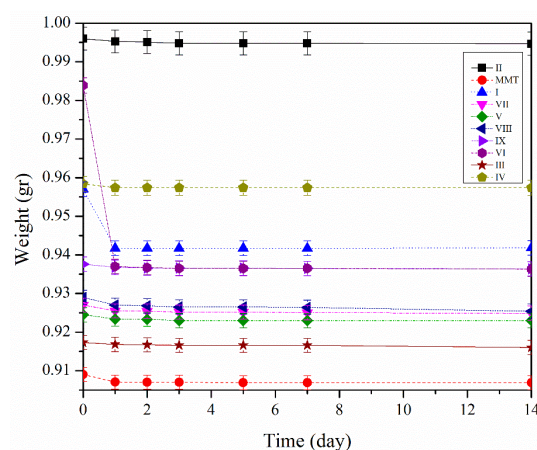
(a)
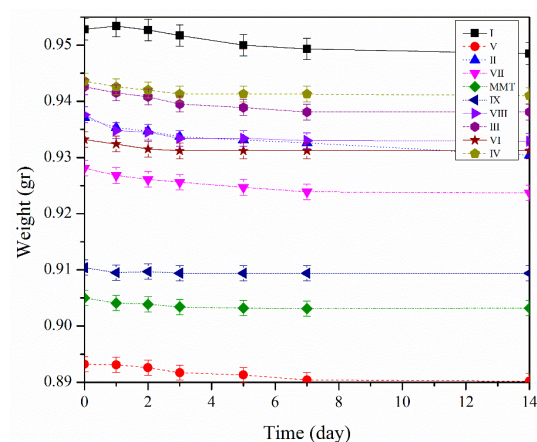
(b)

Fig. 14. Weight loss of (I–IX & MMT) membranes pressed under 50 bar which conditioned in (a) NaOH (pH = 13) & (b) H_2SO_4 (pH = 2) solutions as a function of immersion time.
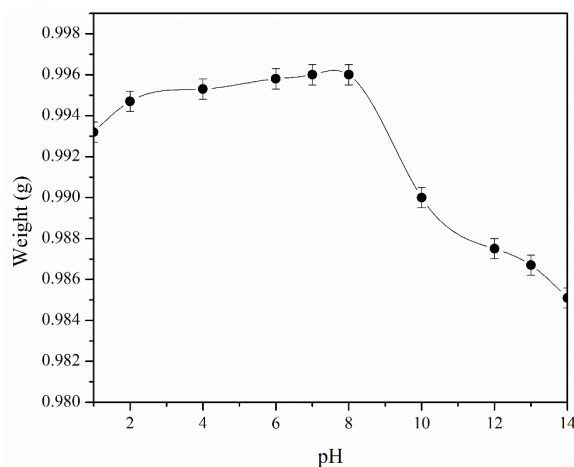
Fig. 15. Weight loss of IX, VIII and VI membranes pressed under 50 bar immersed in acidic and alkaline media prepared using H_2SO_4 and NaOH, respectively as a function of pH.

3.2.8. Mercury porosimetry

Pore diameter and pore size distribution of membrane IX pressed under 50 bar as a function of cumulative and relative pore volume are shown in Fig. 16. According to the results, the membrane is composed of micro and nano-sized pores. Fig. 16 indicates that, ~75% of pores are in the 14–21 nm size range. Also, pores with diameters in the range of 1–3.3 µm, can be observed. As a result, membrane permeability would be improved by the porous structure comprising both inter-particular pores and the pores generated due to PEG decomposition [38].

3.2.9. Surface morphology

Membrane surface morphology and structural analysis was characterized using SEM micrographs. Figs. 17a and b show the surface and cross-section view of membrane No. IX as the optimal membrane. As can be seen, membrane presents a highly porous structure and pores are randomly shaped. The porous structure devoid of cracks, defects and impurities is the final product. Also, particles are attached through intergranular contact and formation of particle boundaries can be observed. It is reported that, <1 µm pores can be generated through impurities melting or structure contracting during sintering process. While, >1 µm pores would be generated through PEG decomposition [38]. Furthermore, Figs. 18a and b show the surface and cross-section view of the fouled membrane No. IX loaded by dye particles after 24 h of filtration. It can obviously be seen that the surface porosity decreased and the surface became smooth which can be attributed to dye penetration into the pores. Covering the top and inside of the structure led to pore blocking during filtration which confirm the membrane flux decline behavior shown in Fig. 11.

3.2.10. Mechanical strength

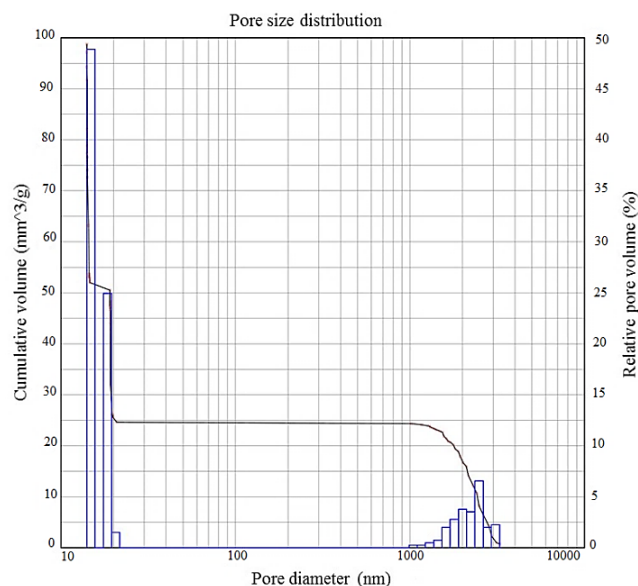Mechanical resistance of IX membrane as the optimal sample was measured using a compressive force. It

Fig. 16. Pore size distribution of membrane No. IX pressed under 50 bar as a function of intruded mercury volume using mercury intrusion porosimetry analysis.

was found that the initial membrane exhibited 8.13 MPa mechanical strength which decreased to 7.9 MPa after 24 h of dye filtration. As can be seen, the membrane mechanical strength did not change significantly.

Symbols

A — Absorbance
ε — Molar absorptivity (molar extinction) coefficient (L·mol^{-1}·cm^{-1})
l — Length of light path (cm)
c — Solution concentration (mol·L^{-1})
V_{op} — Membrane open pore volume (cm^3)
V_a — Membrane apparent volume (cm^3)
m_s — Membrane weight after water absorption (g)
m_d — Initial membrane weight (g)
J — Flux (L·m^{-2}·h^{-1})
Q_w — Permeate volume (L)
Δt — Sampling time (h)
A_m — Membrane specific surface area (m^2)
L_p — Membrane permeability (L·m^{-2}·h^{-1}·bar^{-1})
Δp — Transmembrane pressure (bar)
R — Retention rate
C_p — Permeate concentration (mol·L^{-1})
C_0 — Feed concentration (mol·L^{-1})
C_m — Solute concentration on membrane surface (mol·L^{-1})
k — Mass transfer coefficient (m·s^{-1})
R_{int} — Intrinsic retention

4. Conclusions

Low-cost flat ceramic MF membranes have been fabricated using natural clay minerals mixed with PEG as the binder through uniaxial pressing under low pressures in the 25–150 bar range. XRF analysis of raw minerals
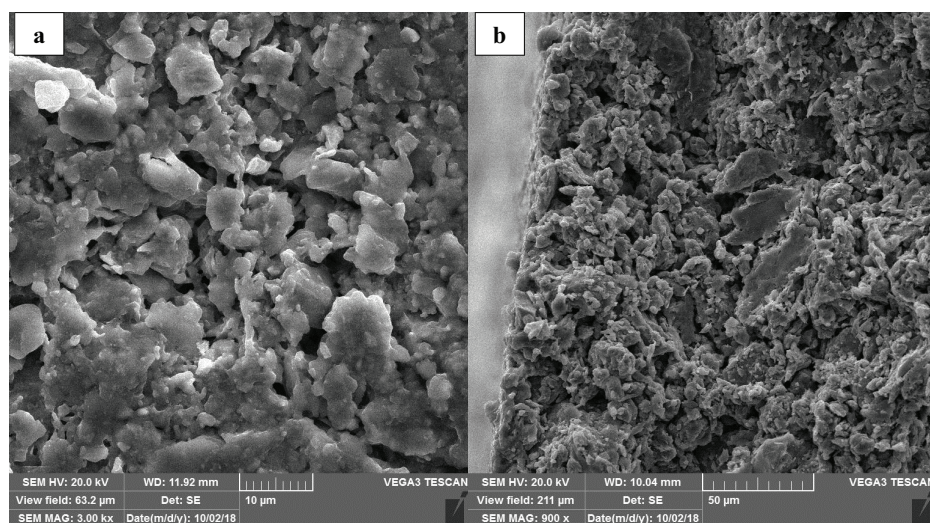
Fig. 17. (a) Surface & (b) cross-section view of SEM micrographs of initial membrane No. IX fabricated under optimal condition.
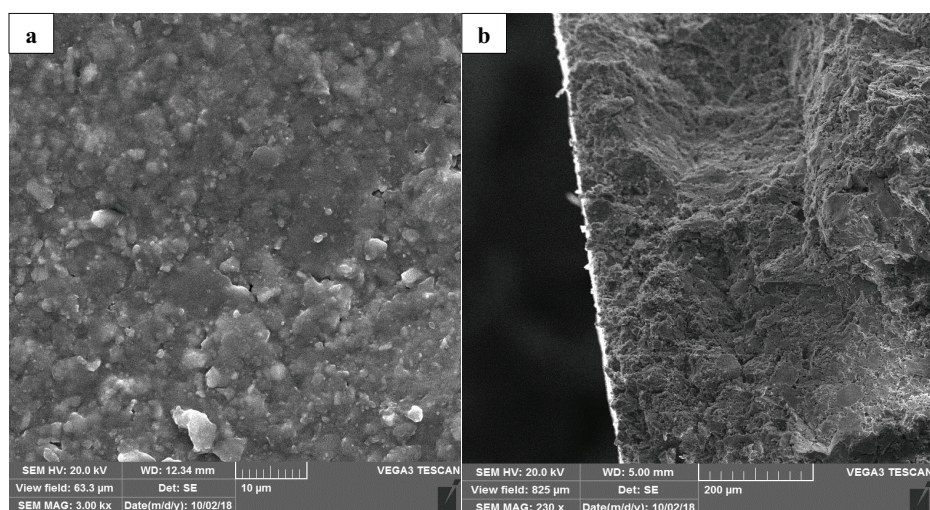

Fig. 18. (a) Surface & (b) cross-section view of SEM micrographs of membrane No. IX fabricated under optimal condition after 24 h of filtration.

revealed that samples were mainly composed of SiO_2 and Al_2O_3. PSD analysis indicated that particles were <6 μm. Increasing the pressing pressure led to porosity and water flux declination. Water flux and dye retention tests were performed under 0.1 bar transmembrane pressure through controlling the height of water above the membrane. According to the results, membrane No. IX pressed under 50 bar was selected as the optimal sample. The membrane with 27% porosity composed of 75% pore size in 14–21 nm and 25% in 1–3.3 μm range, represented 98% anionic and 93% nonionic dye retention for 35 ppm dye solutions. Furthermore, the membrane showed a promising chemical stability in acidic and alkaline media (<1% weight loss) and 10.5% radial shrinkage. The as-prepared membrane can be a perfect candidate for anionic and nonionic dye clarification with excellent retention and economic treatment of textile wastewaters even in harsh acidic and alkaline media.

References

[1] K. Shafiei, M. Kazemimoghaddam, T. Mohammadi, S. Ghanbari Pakdehi, An investigation on manufacturing of alumina microfiltration membranes, Desal. Water Treat., 53 (2015) 2429–2436.
[2] K.K.O. Silva, C.A. Paskocimas, F.R. Oliveira, J.H. Nascimento, A. Zille, Development of porous alumina membranes for treatment of textile effluent, Desal. Water Treat., 57 (2016) 2640–2648.
[3] A. Bayat, H.R. Mahdavi, M. Kazemimoghaddam, T. Mohammadi, Preparation and characterization of γ-alumina ceramic ultrafiltration membranes for pretreatment of oily wastewater, Desal. Water Treat., 57 (2016) 24322–24332.
[4] Z. Sadeghian, F. Zamani, S. Ashrafizadeh, Removal of oily hydrocarbon contaminants from wastewater by γ-alumina nanofiltration membranes, Desal. Water Treat., 20 (2010) 80–85.

[5] R. Terpstra, B. Bonekamp, H. Veringa, Preparation, characterization and some properties of tubular alpha alumina ceramic membranes for microfiltration and as a support for ultrafiltration and gas separation membranes, Desalination, 70 (1988) 395–404.

[6] M. Shokri Doodeji, M.M. Zerafat, M.H. Yousefi, S. Sabbaghi, Effect of OH-treatment of PDMS on rejection in hybrid nanofiltration membranes for desalination, Desalination, 426 (2018) 60–68.

[7] M. Khalili, S. Sabbaghi, M.M. Zerafat, Preparation of ceramic γ-Al$_2$O$_3$-TiO$_2$ nanofiltration membranes for desalination, Chem. Pap., 69 (2015) 309–315.

[8] M. Shokri Doodeji, M.M. Zerafat, O. Nejadian, Fabrication and charge modification of ceramic membranes using copper Nanoparticles for desalination, J. Nanoanalysis., (2017).

[9] T. Van Gestel, C. Vandecasteele, A. Buekenhoudt, C. Dotremont, J. Luyten, R. Leysen, B. Van der Bruggen, G. Maes, Salt retention in nanofiltration with multilayer ceramic TiO$_2$ membranes, J. Membr. Sci., 209 (2002) 379–389.

[10] A. Alem, H. Sarpoolaky, M. Keshmiri, Titania ultrafiltration membrane: preparation, characterization and photocatalytic activity, J. Eur. Ceram. Soc., 29 (2009) 629–635.

[11] A. Ayral, C. Balzer, T. Dabadie, C. Guizard, A. Julbe, Sol-gel derived silica membranes with tailored microporous structures, Catal. Today, 25 (1995) 219–224.

[12] G.-T. Lim, H.-G. Jeong, I.-S. Hwang, D.-H. Kim, N. Park, J. Cho, Fabrication of a silica ceramic membrane using the aerosol flame deposition method for pretreatment focusing on particle control during desalination, Desalination, 238 (2009) 53–59.

[13] A. Larbot, L. Gazagnes, S. Krajewski, M. Bukowska, W. Kujawski, Water desalination using ceramic membrane distillation, Desalination, 168 (2004) 367–372.

[14] N. Saffaj, M. Persin, S.A. Younsi, A. Albizane, M. Cretin, A. Larbot, Elaboration and characterization of microfiltration and ultrafiltration membranes deposited on raw support prepared from natural Moroccan clay: application to filtration of solution containing dyes and salts, Appl. Clay Sci., 31 (2006) 110–119.

[15] F. Bouzerara, A. Harabi, S. Condom, Porous ceramic membranes prepared from kaolin, Desal. Water Treat., 12 (2009) 415–419.

[16] S. Foorginezhad, M.M. Zerafat, Microfiltration of cationic dyes using nano-clay membranes, Ceram. Int., 43 (2017) 15146–15159.

[17] J. Bai, Fabrication and properties of porous mullite ceramics from calcined carbonaceous kaolin and α-Al$_2$O$_3$, Ceram. Int., 36 (2010) 673–678.

[18] S. Masmoudi, A. Larbot, H. El Feki, R.B. Amar, Elaboration and properties of new ceramic microfiltration membranes from natural and synthesized apatite, Desalination, 190 (2006) 89–103.

[19] Y. Dong, X. Feng, D. Dong, S. Wang, J. Yang, J. Gao, X. Liu, G. Meng, Elaboration and chemical corrosion resistance of tubular macro-porous cordierite ceramic membrane supports, J. Membr. Sci., 304 (2007) 65–75.

[20] L. Wang, C. Wang, Y. Mao, E. Du, X. Xu, Eutrophic lake water treatment using a diatomite porous ceramic membrane, Desal. Water Treat., 53 (2015) 586–592.

[21] M.-M. Lorente-Ayza, M. Orts, V. Pérez-Herranz, S. Mestre, Role of starch characteristics in the properties of low-cost ceramic membranes, J. Eur. Ceram. Soc., 35 (2015) 2333–2341.

[22] N. Kouras, A. Harabi, F. Bouzerara, L. Foughali, A. Policicchio, S. Stelitano, F. Galiano, A. Figoli, Macro-porous ceramic supports for membranes prepared from quartz sand and calcite mixtures, J. Eur. Ceram. Soc., 37 (2017) 3159–3165.

[23] B. Nandi, R. Uppaluri, M. Purkait, Preparation and characterization of low cost ceramic membranes for micro-filtration applications, Appl. Clay Sci., 42 (2008) 102–110.

[24] P.B. Belibi, M. Nguemtchouin, M. Rivallin, J.N. Nsami, J. Sieliechi, S. Cerneaux, M. Ngassoum, M. Cretin, Microfiltration ceramic membranes from local Cameroonian clay applicable to water treatment, Ceram. Int., 41 (2015) 2752–2759.

[25] S. Bose, C. Das, Sawdust: From wood waste to pore-former in the fabrication of ceramic membrane, Ceram. Int., 41 (2015) 4070–4079.

[26] S. Mondal, M.K. Purkait, S. De, Advances in Dye Removal Technologies, Springer, 2018.

[27] A. Kausar, M. Iqbal, A. Javed, K. Aftab, H.N. Bhatti, S. Nouren, Dyes adsorption using clay and modified clay: A review, J. Mol. Liq., 256 (2018) 395–407. (article in press)

[28] P. Kumar, T.T. Teng, S. Chand, K.L. Wasewar, Fenton oxidation of carpet dyeing wastewater for removal of COD and color, Desal. Water Treat., 28 (2011) 260–264.

[29] P. Sathe, M.T.Z. Myint, S. Dobretsov, J. Dutta, Removal and regrowth inhibition of microalgae using visible light photocatalysis with ZnO nanorods: A green technology, Sep. Purif. Technol., 162 (2016) 61–67.

[30] H. Soni, N. Kumar, K. Patel, R.N. Kumar, Photo catalytic efficiency and kinetic studies of ZnO nanoparticles for the removal of basic dye Rhodamine B, Desal. Water Treat., 57 (2016) 19857–19864.

[31] C. Jia, X. Li, Z. Liu, B. Xu, S. Yao, H. Song, Adsorption process and mechanism for furfural separation with macroporous resin, Desal. Water Treat., 56 (2015) 2214–2224.

[32] L. Zhuang, G. Wang, K. Yu, C. Yao, Enhanced adsorption of anionic dyes from aqueous solution by gemini cationic surfactant-modified diatomite, Desal. Water Treat., 51 (2013) 6526–6535.

[33] J. Mulder, Basic principles of membrane technology, Springer Science and Business Media, 2012.

[34] B. Ghouil, A. Harabi, F. Bouzerara, B. Boudaira, A. Guechi, M.M. Demir, A. Figoli, Development and characterization of tubular composite ceramic membranes using natural alumino-silicates for microfiltration applications, Mater. Charact., 103 (2015) 18–27.

[35] S. Emani, R. Uppaluri, M.K. Purkait, Microfiltration of oil–water emulsions using low cost ceramic membranes prepared with the uniaxial dry compaction method, Ceram. Int., 40 (2014) 1155–1164.

[36] A. Bouazizi, S. Saja, B. Achiou, M. Ouammou, J. Calvo, A. Aaddane, S.A. Younssi, Elaboration and characterization of a new flat ceramic MF membrane made from natural Moroccan bentonite. Application to treatment of industrial wastewater, Appl. Clay Sci., 132 (2016) 33–40.

[37] L. Palacio, Y. Bouzerdi, M. Ouammou, A. Albizane, J. Bennazha, A. Hernández, J. Calvo, Ceramic membranes from Moroccan natural clay and phosphate for industrial water treatment, Desalination, 245 (2009) 501–507.

[38] C.-Y. Yun, W.-Y. Kim, D.-J. Son, D.-G. Kim, D. Chang, S.-O. Chang, Y. Sunwoo, K.-H. Hong, Fabrication of tubular-type MF ceramic membrane with enhanced permeability by addition of PMMA in the support and evaluation of physical characteristics for wastewater treatment, Ceram. Int., 41 (2015) 10788–10794.

[39] M. Mouiya, A. Abourriche, A. Bouazizi, A. Benhammou, Y. El Hafiane, Y. Abouliatim, L. Nibou, M. Oumam, M. Ouammou, A. Smith, Flat ceramic microfiltration membrane based on natural clay and Moroccan phosphate for desalination and industrial wastewater treatment, Desalination, 427 (2018) 42–50.

[40] S. Saja, A. Bouazizi, B. Achiou, M. Ouammou, A. Albizane, J. Bennazha, S.A. Younssi, Elaboration and characterization of low-cost ceramic membrane made from natural Moroccan perlite for treatment of industrial wastewater, J. Environ. Chem. Eng., 6 (2018) 451–458.

[41] A. Majouli, S.A. Younssi, S. Tahiri, A. Albizane, H. Loukili, M. Belhaj, Characterization of flat membrane support elaborated from local Moroccan Perlite, Desalination, 277 (2011) 61–66.

[42] H.K. Gordon, R. Chambers, The particle size of acid dyes and their diffusibility into living cells, J. Cell. Comp. Physiol., 17 (1941) 97–108.

[43] S. Bose, C. Das, Preparation and characterization of low cost tubular ceramic support membranes using sawdust as a pore-former, Mater. Lett., 110 (2013) 152–155.

[44] D. Vasanth, G. Pugazhenthi, R. Uppaluri, Fabrication and properties of low cost ceramic microfiltration membranes for separation of oil and bacteria from its solution, J. Membr. Sci., 379 (2011) 154–163.

[45] M. Issaoui, L. Limousy, B. Lebeau, J. Bouaziz, M. Fourati, Design and characterization of flat membrane supports elaborated from kaolin and aluminum powders, C.R. Chim., 19 (2016) 496–504.

[46] B. Chakrabarty, A. Ghoshal, M. Purkait, SEM analysis and gas permeability test to characterize polysulfone membrane prepared with polyethylene glycol as additive, J. Colloid Interface Sci., 320 (2008) 245–253.

[47] C.-W. Lee, H.-S. Kang, Y.-H. Chang, Y.-M. Hahm, Thermotreatment and chemical resistance of porous alumina membrane prepared by anodic oxidation, Korean J. Chem. Eng., 17 (2000) 266–272